

Angle-Resolved Resonant Photoemission as a Probe of Spatial Localization and Character of Electron States

S. L. Molodtsov,^{1,*} M. Richter,² S. Danzenbächer,¹ S. Wieling,¹ L. Steinbeck,^{2,3} and C. Laubschat¹

¹*Institut für Oberflächenphysik und Mikrostrukturphysik, TU Dresden, D-01062 Dresden, Germany*

²*Max-Planck-Arbeitsgruppe "Elektronensysteme," TU Dresden, D-01062 Dresden, Germany*

³*Department of Physics, University of York, York YO1 5DD, United Kingdom*

(Received 24 June 1996)

Resonant photoemission (PE) in the angle-resolved mode is proposed as a method to determine the spatial localization and the angular momentum character of valence band states from *on-resonance* PE signals across the Brillouin zone. This technique is applied to study ordered films of La metal. The obtained experimental data agree well with the results of band-structure calculations and related eigenvector analysis. [S0031-9007(96)02023-6]

PACS numbers: 79.60.Bm, 71.20.Eh

Apart from binding energy, symmetry and spatial localization are main fundamental parameters to characterize electron states in solids. While for core levels these parameters are easily defined, for valence bands the situation is complicated due to the hybridization and \mathbf{k} dependence of the electron states. Particularly for valence states, however, a detailed information on symmetry and spatial localization is crucial for a deeper insight into the chemical, electronic, and magnetic properties of the materials.

Experimentally, this problem is usually attacked by exploiting the properties of the dipole-matrix element in photoemission (PE), x-ray absorption, or x-ray emission spectroscopies [1]. For certain geometries, selection rules allow one to extract data on the symmetry of the states and a rough determination of the angular momentum character becomes possible. Unfortunately, due to the linear dependence of the dipole operator on the space coordinate \vec{r} these methods are less sensitive to spatial localization. In this respect, Auger spectroscopy is much more favorable due to the $1/r$ dependence of the Coulomb interaction ruling the related matrix element. However, in a classical Auger process the signals are energetically strongly broadened by lifetime and multiplet splittings due to the core holes involved.

The latter restriction may be overcome by the application of resonant PE. This experimental technique, which has been successfully applied to transition metals [2], rare earth's [3], actinides [4], and high-temperature superconductors [5], is based on the configuration mixing of two different states: a continuum final state $|f(\varepsilon, \mathbf{k})\rangle$ represent-

ing the excited photoelectron and a hole in the valence band with quasimomentum $\hbar\mathbf{k}[\mathbf{k} = (k, \nu)$, where ν is the valence band index] and a discrete intermediate state $|m\rangle$ created by the transition of a core electron to a localized conduction state. The state $|m\rangle$ can decay into the final state via an Auger process. Since the probability of transitions into the intermediate state varies dramatically when tuning the photon energy ε across a core level threshold, large variations of the photoionization cross section are obtained known as Fano-Beutler resonance in atomic physics [6]. Recently, it has been observed experimentally [7] that in resonant PE electron momentum is conserved as in nonresonant PE. This fact may be understood if (i) the contribution from phonon assisted processes can be neglected and (ii) the intermediate state decays into the final state before its coherency is lost. For a generalization of the atomic theory [8] to \mathbf{k} -dependent states, we introduce three matrix elements ruling the effect: the dipole transition matrix element between the initial state $|i\rangle$ and the final state, $T(\varepsilon, \mathbf{k}) = \langle f(\varepsilon, \mathbf{k}) | \hat{T}_D | i \rangle$, where \hat{T}_D is the dipole operator; the dipole transition matrix element between the initial and the intermediate state, $T_0 = \langle m | \hat{T}_D | i \rangle$, and the Auger matrix element between the intermediate state and the final state, $A(\varepsilon, \mathbf{k}) = \langle f(\varepsilon, \mathbf{k}) | \hat{T}_A | m \rangle$, where \hat{T}_A is the Auger operator.

The \mathbf{k} dependence of A is strong due to differences in the spatial localization of the valence hole states. The \mathbf{k} dependence of T , on the other hand, arises from the particular angular momentum composition of these states. The cross section $\sigma(\varepsilon, \mathbf{k})$ is given in analogy to Ref. [8] by

$$\sigma(\varepsilon, \mathbf{k}) \propto \left| T(\varepsilon, \mathbf{k}) + \frac{A(\varepsilon, \mathbf{k})}{\varepsilon - \varepsilon_0 - i\Gamma} \left[T_0 + \int d\varepsilon' \frac{\sum_{\mathbf{k}'} A^*(\varepsilon', \mathbf{k}') T(\varepsilon', \mathbf{k}')}{\varepsilon - \varepsilon' - i0} \right] \right|^2 = \left| T(\varepsilon, \mathbf{k}) + \frac{A(\varepsilon, \mathbf{k}) \tilde{T}_0(\varepsilon)}{\varepsilon - \varepsilon_0 - i\Gamma} \right|^2, \quad (1)$$

where ε_0 is the resonance energy and Γ is the inverse lifetime of the intermediate state. Interference of three channels is considered in Eq. (1): (i) direct PE from the valence band; (ii) transition into $|m\rangle$ followed by decay

into $|f\rangle$; (iii) virtual transition into a final state $|f'\rangle$ followed by transition to $|m\rangle$ and decay. The third channel, responsible for the Fano line shape in atomic theory, does not change the \mathbf{k} dependence of the resonant term. At the

resonance, $\varepsilon = \varepsilon_0$,

$$\sigma^{\text{on-res}}(\mathbf{k}) \propto |T(\varepsilon_0, \mathbf{k}) + iA(\varepsilon_0, \mathbf{k})\tilde{T}_0(\varepsilon_0)/\Gamma|^2.$$

Assuming $|A(\varepsilon_0, \mathbf{k})\tilde{T}_0(\varepsilon_0)/\Gamma| \gg |T(\varepsilon_0, \mathbf{k})|$, we get

$$\sigma^{\text{on-res}}(\mathbf{k}) \approx \text{const}|A(\varepsilon_0, \mathbf{k})|^2, \quad (2)$$

and the state dependence of the measured on-resonance intensities may be explained by the single matrix element $A(\varepsilon_0, \mathbf{k})$ [9], which is intimately related to the spatial localization of the final valence-band hole with respect to the intermediate state. In turn, the spatial localization depends on the angular momentum character of the states. Thus, this simple relationship may be used to sample the angular momentum character of valence-band states, exploiting the \mathbf{k} -dependent intensity variations of on-resonance photoemission signals.

In the present Letter, we report on an angle-resolved photoemission (ARPE) study of the valence bands of La metal measured at the $4d \rightarrow 4f$ excitation. The experimental data are compared to results of LCAO band-structure calculations. It is shown that the on-resonance ARPE-intensities are proportional to the localized part of the La $5d$ contributions to the squared Bloch wave function amplitude. In this way, a quantitative mapping of the angular momentum character of the valence states as a function of electron momentum (and band index) \mathbf{k} is achieved.

Films of La metal (80 Å thick) were grown *in situ* onto a W(110) substrate by thermal deposition from La drops molten on Ta strips. The pressure during evaporation was always better than 3×10^{-10} Torr. The deposited films were annealed at a temperature of about 600 °C until a characteristic sharp hexagonal LEED pattern indicated the formation of an ordered (0001) surface of α -La, which is the stable *dhcp* phase at room temperature.

The angle-resolved experiments were performed at the HE-PGM-2 beam line of BESSY using a rotatable hemispherical electron energy analyzer (ARIES-VSW, 1° angle resolution). The photon energies for the $4d \rightarrow 4f$ on- and off-resonance excitation were set to 117 and 112 eV, respectively, as obtained from x-ray absorption measurements performed in the electron yield mode. The dispersion of electron states within the Γ - A - H - K plane in the Brillouin zone (BZ) of α -La was mapped changing only the polar angle (Θ) of analyzing. The azimuthal angle was kept constant along the Γ - K direction as was determined from the LEED pattern. At each polar angle both on- and off-resonance spectra were recorded. The relative small difference of the corresponding photon energies leads to only minor inaccuracies in sampling of particular points in reciprocal space that lies within the error bars of the angle resolution of the experiment. Experimental spectra were least-squares fitted by a series of Lorentzians convoluted by a Gaussian to account for finite experimental resolution.

The experimental results were compared to band-structure calculations for *dhcp* La performed within the

scalar-relativistic version of the method of optimized linear combination of atomic orbitals [10]. In this method, the Bloch wave function $|\mathbf{k}\rangle$ is composed of overlapping atomiclike orbitals $|nlmi\rangle$ centered at atomic sites i with coordinates \vec{R}_i , $|\mathbf{k}\rangle = \sum_{nlmi} C_{nlmi}(\mathbf{k})e^{i\vec{k}\cdot\vec{R}_i}|nlmi\rangle$. Here, l and m denote angular momentum and magnetic quantum numbers, respectively. In our specific case, the atomic states are $6s$, $6p$, and $5d$. Note that for each l only one specific principal quantum number n is considered. The charge density related to each occupied state $|\mathbf{k}\rangle$ is

$$\rho(\mathbf{k}) = \sum_{nlmi} \sum_{n'l'm'i'} C_{nlmi}(\mathbf{k})C_{n'l'm'i'}^*(\mathbf{k}) \times e^{i\vec{k}\cdot(\vec{R}_i - \vec{R}_{i'})} \langle \vec{r} | nlmi \rangle \langle n'l'm'i' | \vec{r} \rangle$$

and can be decomposed into overlap contributions $i \neq i'$ and net or on-site contributions $i = i'$. The latter represent the spatially localized part of the charge density and may be further decomposed into contributions related to a specific angular momentum l :

$$\rho_{nli}^{\text{net}}(\mathbf{k}) = \sum_m C_{nlmi}(\mathbf{k})C_{nlmi}^*(\mathbf{k}) \times \langle \vec{r} | nlmi \rangle \langle nlmi | \vec{r} \rangle.$$

Terms $m \neq m'$ and $l \neq l'$ do not contribute to a spherically averaged net charge density. The quantity $N_{nli}^{\text{net}}(\mathbf{k}) = \sum_m C_{nlmi}(\mathbf{k})C_{nlmi}^*(\mathbf{k})$ we call the nl -net character of the state $|\mathbf{k}\rangle$.

The off-resonance spectra ($h\nu = 112$ eV) taken at various Θ 's were separately analyzed in order to assign the experimental data to particular points in the BZ. Three main features can be clearly seen from the spectra shown in Fig. 1: A low-intensity high binding-energy (BE) peak **a** shows dispersion toward the Fermi energy (E_F) with increasing angle of analyzing. In contrast to peak **a**, structure **b** moves first toward E_F ($\Theta < 5^\circ$), then back to high BE's ($5^\circ < \Theta < 8^\circ$), and finally again in the direction to the Fermi level ($\Theta > 8^\circ$). The third structure **c** is not seen for small polar angles. This feature intersects E_F at $\Theta \approx 5^\circ$ and stays close to E_F (≈ 0.2 eV BE) for larger Θ 's. Both features **b** and **c** are characterized by higher PE intensities as compared to that of structure **a**.

Since the perpendicular component of the momentum of emitted electrons ($\hbar k_\perp$) is not conserved in PE, the experimental results were compared with theoretical bands calculated within the Γ - A - H - K plane at various fixed values of k_\perp . This procedure seems to be justified in the present case of analyzing nearly normal-emission electrons excited at high kinetic energies, where \vec{k} does not significantly change within the whole range of polar angle variation. An optimum agreement between the experimental data and the results of theoretical calculations was achieved for $k_\perp^* = 0.75\pi/c$, where c is the lattice constant. The experimental results are compared to the calculated band dispersions in the inset of Fig. 1. Here, the positions of the points Δ^* and P^* in \vec{k} space are defined as $\Gamma + k_\perp^*$ and $K + k_\perp^*$, respectively. Three

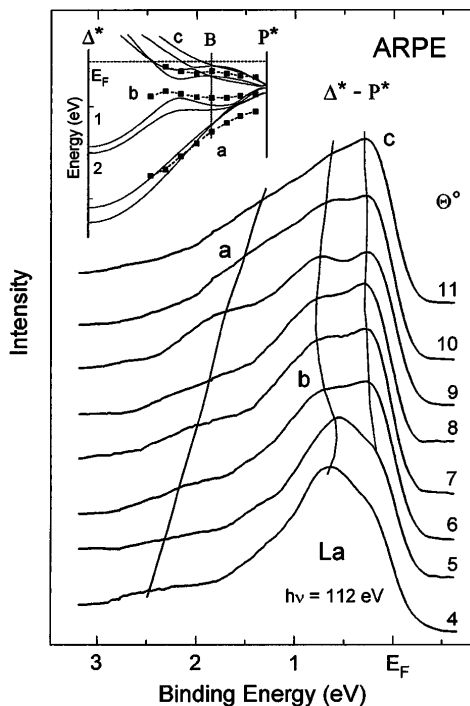


FIG. 1. Off-resonance angle-resolved PE spectra taken with $h\nu = 112$ eV at various polar angles along the $\Delta^* - P^*$ direction in the BZ of $dhcp$ La metal (see text). A comparison between experimental data and results of LCAO band-structure calculations is shown in the inset to the figure.

groups of occupied bands, which can be assigned to the experimental features **a**, **b**, and **c**, can be distinguished in the calculated valence-band structure. The nearly degenerated bands assigned to each feature are almost equivalent in symmetry. Thus, the whole following analysis is done for net characters summed over the occupied bands in each group and over all atomic sites in the elementary cell.

The different character of the electron states leads to a distinct resonant enhancement of signals from different valence bands. As an example, in Fig. 2(a) we show on- and off-resonance spectra taken at a polar angle 8° that corresponds to a point in the $\Delta^* - P^*$ direction marked by **B** in Fig. 1 (inset). The PE spectra are normalized to photon flux. Among the three peaks, structure **c** reveals the strongest resonant enhancement. The PE weight **b** resonates to a less extent, while feature **a** shows almost no resonant effect.

To illustrate the reason for this different resonant behavior we have calculated the densities $\rho(\mathbf{k})$ for two particular eigenstates at the point **B**. Figure 2(b) shows charge densities related to the experimental features **a** and **b**, respectively. We have chosen a $14 \text{ a.u.} \times 14 \text{ a.u.}$ cut in the x - z plane (perpendicular to the hexagonal plane) containing three La atoms. The atomic positions can be identified by the high-density peaks (feature **a**). The density in the interstitial region is rather flat for feature **a**, whereas for feature **b** each atomic site is surrounded

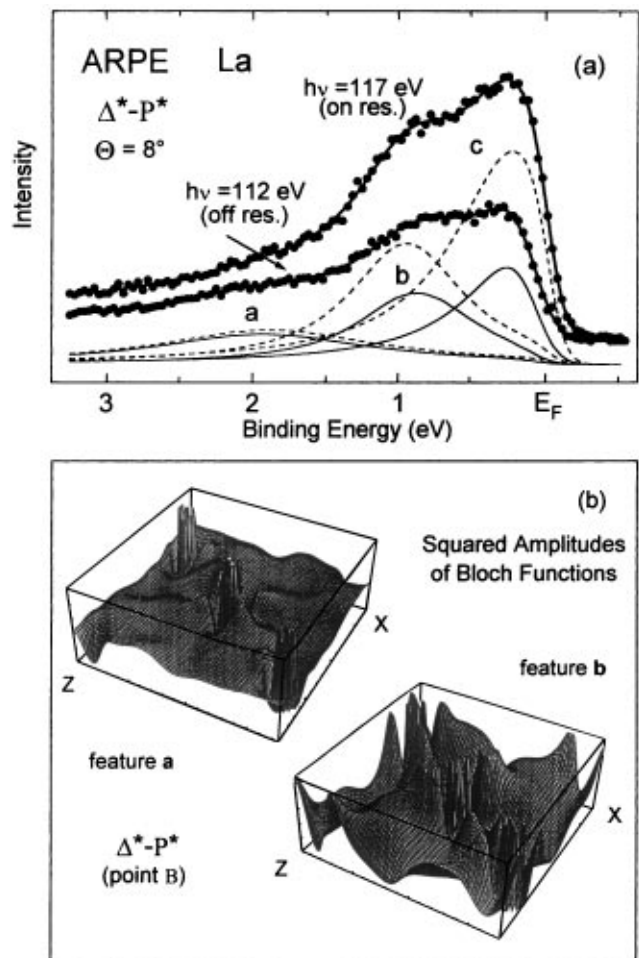


FIG. 2. (a) On- and off-resonant PE spectra of La-metal taken with $h\nu = 117$ eV and $h\nu = 112$ eV, respectively, at the point **B** ($\Theta = 8^\circ$) in the $\Delta^* - P^*$ direction. Subspectra represent results of a least-squares-fit analysis of on-resonance (dashed) and off-resonance (solid) intensities. (b) Densities $\rho(\mathbf{k})$ at the **B** point for bands related to feature **a** (lowest band in the inset in Fig. 1) and feature **b** (fourth band from the bottom), respectively. Note, that bands related to feature **c** are characterized by charge densities that are qualitatively similar to those of bands contributing to feature **b**. The densities are given in arbitrary units, peaks are cut to allow for sufficient resolution.

by four bumps at a distance of about 2 a.u. These bumps arise from a large d_{xz} -net content in the related wave functions. In contrast, the flat density for feature **a** consists mainly of sp -net and overlap contributions. Thus, the respective states are characterized by different degrees of spatial localization that result in distinct resonant enhancements of the corresponding PE features.

As might be expected from Eq. (2) the \mathbf{k} -resolved variations of on-resonance ARPE intensities are mainly caused by the squared matrix element $|A(\epsilon_0, \mathbf{k})|^2$, which is dominated by the La $5d$ -net charge density contribution for the following reason: Considering atomic states, the positions of the outermost radial charge density maxima mainly depend on the principle quantum number. They

are at distances from the nuclei of 3.3, 3.4, and 2.2 a.u. for $l = 0, 1,$ and 2 ($6s, 6p,$ and $5d$), respectively, in La. Therefore, the $5d$ contribution to each state is much more localized and closer to the $n = 4$ states than the $6s$ and $6p$ contributions, and $|A(\epsilon_0, 5d)| \gg |A(\epsilon_0, 6s6p)|$. Note, that the maxima of radial charge density of both the $4d$ core states and the $4f$ states lie at about 0.7 a.u.

The experimentally derived intensity variations together with the calculated occupied $N_{5d}^{\text{net}}(\mathbf{k})$ are shown in Fig. 3. The jumps of the curve plotted for feature **c** are caused by the Fermi-level crossings of the contributing bands (see inset in Fig. 1). All these individual bands have a d -net character of approximately 70% at any analyzed point along the Δ^*-P^* direction. In contrast to the bands contributing to feature **c**, bands associated with structures **a** and **b** are fully occupied. The two bands of feature **a** are characterized by almost pure s -character in the region of the Δ^* point, while they have predominantly d -net character ($\approx 60\%$) close to the P^* point. The two bands of structure **b** reveal a higher net contribution of d symmetry, which amounts to more than 35% close to Δ^* ; it increases up to almost 60% along the Δ^*-P^* direction and reduces to $\approx 55\%$ close to the border of the BZ.

The on-resonance PE intensities of peaks **a**, **b**, and **c** are shown in Fig. 3 by solid triangles, circles, and squares, respectively. The experimental values were normalized to incident photon flux. To take into account the constant appearing in Eq. (2), an additional normalization to the d -net character of peak **c** has been done at the **B** point, where all three photoemission structures **a**, **b**, and **c** are well resolved and can be easily fitted. An excellent

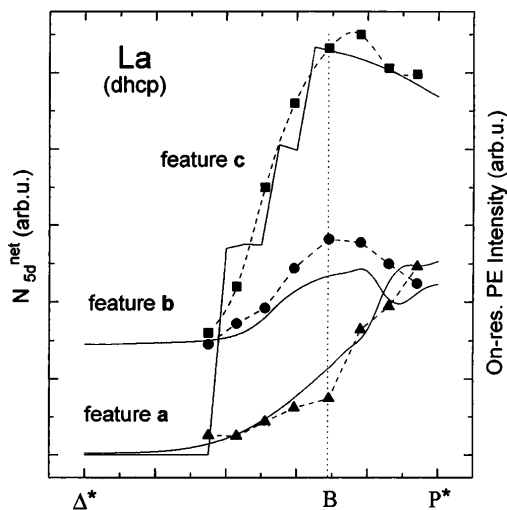


FIG. 3. Occupied $5d$ -net characters N_{5d}^{net} of the three valence-band structures (solid lines) in comparison to normalized on-resonance PE intensities of features **a** (triangles), **b** (circles), and **c** (squares) measured along the Δ^*-P^* direction.

agreement is obtained between the experimental results and the calculated data. The character dependence of $T(\epsilon, \mathbf{k})$, which is similar but less pronounced than that of $A(\epsilon, \mathbf{k})$, does obviously not disturb the linear relation between on-resonance intensities and d -net character. Thus, the results presented in Fig. 3 demonstrate that the applied method of ARPE can serve as a tool to map the most localized contribution to the character of valence states over the BZ.

In summary, a new application of resonant PE in the angle-resolved mode is presented, which allows to map the valence state angular momentum character as a function of quasimomentum and band index. The proposed technique is capable to provide a wealth of information both on the symmetry of electron states and the degree of their spatial localization. Thereat, only on-resonance intensities are considered. Here, this method was applied to study the valence bands in ordered films of La metal. It may be extensively used for investigations of a wide range of materials which exhibit a Fano-type resonant behavior, including lanthanides, actinides, and their compounds as well as late transition metal systems.

This work was supported by the Bundesministerium für Bildung und Forschung (BMBF), Project No. 056250DA, and the Deutsche Forschungsgemeinschaft, Project No. LA 655/3-1. We thank V. N. Antonov, H. Eschrig, O. Gunnarsson, S. Halilov, and P. M. Oppeneer for valuable discussions. Experimental assistance by the staffs of BESSY and of the Universität Bochum (AG Freund) is gratefully acknowledged.

*On leave from Institute of Physics, St. Petersburg State University, 198904 St. Petersburg, Russia.

- [1] A. Mansour *et al.*, Phys. Rev. Lett. **58**, 614 (1987); E. W. Plummer and W. Eberhardt, Adv. Chem. Phys. **49**, 533 (1995); R. A. Rosenberg *et al.*, Phys. Rev. B **33**, 4034 (1986).
- [2] L. Ley *et al.*, Phys. Rev. B **35**, 2839 (1987).
- [3] C. Laubschat *et al.*, Phys. Rev. Lett. **65**, 1639 (1990).
- [4] B. Reihl *et al.*, Phys. Rev. B **32**, 3530 (1985).
- [5] S. L. Molodtsov *et al.*, Z. Phys. B **92**, 347 (1993); P. Thiry *et al.*, Europhys. Lett. **5**, 55 (1988).
- [6] U. Fano, Phys. Rev. **124**, 1866 (1961).
- [7] C. G. Olson *et al.*, Phys. Rev. Lett. **76**, 4265 (1996).
- [8] C.-O. Almbladh and L. Hedin, in *Handbook on Synchrotron Radiation*, edited by E. E. Koch (North-Holland, Amsterdam, 1983), Vol. 1b.
- [9] This simplifying assumption is not essential if matrix elements A and T are characterized by similar \mathbf{k} dependence.
- [10] M. Richter and H. Eschrig, Solid State Commun. **53**, 529 (1989); H. Eschrig, *Optimized LCAO Method* (Springer-Verlag, Berlin, 1989).